UNIVERSITY OF TARTU

FACULTY OF SCIENCE AND TECHNOLOGY

INSTITUTE OF PHYSICS

Mikk Antsov

Tribological and mechanical characterization of ZnO nanowires

Master thesis (30 EAP)

Supervisors: Leonid Dorogin, PhD

Sergei Vlassov, PhD

Approved for defence .....

Supervisors .....

.....

signature, date

Tartu 2013

Table of Contents

Abbreviations

AFM	Atomic Force Microscopy
EBT	Elastic Beam Theory
MEMS	Microelectromechanical systems
NEMS	Nanoelectromechanical systems
NW	Nanowire
QTF	Quartz Tuning Fork
SEM	Scanning Electron Microscope
VLS	Vapour-liquid-solid

1. INTRODUCTION

Nanowires (NWs) can be defined as 1D crystalline structures with characteristic diameter ranging from 1 nm to 100 nm and unconstrained length. NWs are known to have unique mechanical [1], optical [2] and electrical [3] properties in comparison to the bulk material and have number of promising applications in mechanics [4] electronics [5] and piezotronics [6]. Specifically, since zinc oxide (ZnO) NWs possess piezoelectric and piezoresistive properties [7-11] it is a promising material for energy harvesting microelectromechanical (MEMS) and nanoelectromechanical (NEMS) systems. Considering that fabrication of NW-based electromechanical devices requires precise control over positioning and subsequent behaviour of the NWs, as well as the fact that friction and adhesion can cause failures of NEMS, it is evident, that deeper understanding of NW-surface interaction mechanisms is essential from applicative point of view.

One of the simplest possible physical systems for studies of the mechanical properties consists of a NW upon a flat surface and external manipulator. Various physical phenomena can be investigated in such a system, including elasticity of NW, adhesion and friction between NW and substrate, electrostatic forces [12] and conductivity [13]. However, the state of the art in NW manipulation still exhibits many unknowns in the interpretation of the experimental data. Large scattering of experimental data, lack of theoretical explanations, incomplete models, in some cases unpredictable behaviour of the system are common. NWs inherit some degree of randomly distributed macroscopic properties such as surface defects, contaminations and impurities that promote indefiniteness of the physical system and complicate the interpretation.

Elastically deformed NWs are appealing objects to investigate NW's elastic properties and coupling with other related phenomena such as piezoresistivity, piezoelectricity and friction.

The aim of this thesis is to investigate the mechanical and tribological properties of ZnO experimentally and theoretically. Nanomanipulation techniques are applied for Young modulus measurements and results are used for calculating the friction properties of NWs. Within the framework of the thesis, manipulation experiments are performed and for interpreting the results a script was developed, employing the elastic beam theory (EBT).

The thesis contains three main parts. In the "background" section general information on nanowires is given. Moreover, methods available in literature on measuring tribological

and mechanical properties of nanowires are reviewed. “Materials and methods” section contains experimental details and description of theoretical models employed for tribomechanical measurements. In “Results and discussion” section results of manipulation experiments and theoretical analysis are presented and discussed.

2. AIM OF THE STUDY

The main goal of the study is to propose new more accurate methods for characterising the tribological and mechanical properties of NWs and demonstrate experimentally on ZnO NWs on a flat Si surface. A number of objectives were identified in order to achieve this goal. The primary list of objectives included:

- Conduction of NW bending experiments where ZnO NWs are half-suspended over trenches in Si wafer and measuring their mechanical response;
- Application of EBT based analytical model for Young modulus measurement in the bending experiments;
- Conduction of manipulation measurements on ZnO NWs on flat Si substrate and observation of NWs mechanical response;
- Application of EBT based analytical model for measurement of distributed kinetic friction force between NW and the substrate;
- Elaboration and application of EBT based analytical model for NWs self-balanced by distributed static friction;
- Comparing originally developed model for static friction distribution analysis to previously known models.

3. BACKGROUND

3.1 Nanowires

3.1.1 General information

NWs are now among most important objects in modern science and have number of promising applications in nanotechnology including high-density data storage, electronic and optoelectronic nanodevices, metallic interconnects, nanoelectromechanical systems (NEMS) and others [14]. NWs are ultrafine wires having typical diameter in the range of 1-100 nm and high aspect ratio.

Properties of NWs may be superior in comparison to corresponding bulk material. [15] NWs have increased surface area, enhanced exciton binding energy, diameter-dependent band gap, increased surface scattering for electrons and phonons, and other peculiarities [16]. NWs can be made from a wide range of materials, and can be conductive, semiconducting or dielectric. Semiconductor NWs, such as e.g. those made of Si, ZnO, GaN or InP, generate most interest, as they have demonstrated especially remarkable optical, electronic and magnetic characteristics (for example, Si NWs can guide light around very tight corners [17]). Important advantage of NWs from an applicative point of view is that in contrast to their bulk counterparts, some of the materials parameters, like e.g. thermal conductivity, which are critical for certain applications, can be independently controlled. NWs made of the same material may possess dissimilar properties due to differences in their crystal phase, crystalline size, surface conditions, and aspect ratios, which depend on the synthesis methods and conditions used in their preparation [16].

NWs exhibit extremely high elasticity that allows large degrees of mechanical deformation (up to 6 per cent in tensile strain according to theoretical calculation for very small wire [18]) without cracking or fracture, while thin film can easily generate cracks after applying even smaller strain. Second, the small size of the NWs largely increases the toughness and robustness of the structure so that it is almost fatigue free. Third, a relatively small force is required to induce the mechanical agitation, so that it can be very beneficial for building ultrasensitive devices.

3.1.2 Synthesis

The growth of nanowires from an isotropic medium is relatively simple and straightforward. Uniform nanowires can be easily grown from an anisotropic solid with lengths up to hundreds of micrometres, no matter whether the synthesis is carried out in a vapour or solution phase. For many solids that are characterized by isotropic crystal structures, symmetry breaking is required in the nucleation step to induce anisotropic growth. To this end, a large number of approaches have been explored to lower the symmetry of a seed to produce nanostructures with one dimensional morphologies.
In this part some methods of nanowire synthesis are introduced and a general overview is given. [19]

Direct vapour-phase methods

Although the exact mechanism behind the 1D growth in the vapour phase is still unclear, this method has been explored thoroughly to synthesize whiskers and nanowires from different materials. Most of the synthesis products are oxides due to the fact that oxidation is inevitable because of O_2 in the reaction chamber.

Advantages of vapour-phase methods are its simplicity and ease of construction and operation. A simple overview of the process is as follows: the vapour phase is generated by evaporation other kinds of vapour reactions, then is transported and condensed onto the substrate placed in a lower temperature zone, where the growth starts due to supersaturation of the gaseous precursor. For example, Zhu et al has fabricated Si_3N_4, SiC, Ga_2O_3, and ZnO nanowires by heating commercial powders of these materials. [19, 20]

Indirect vapour-phase methods

Most vapour-phase methods look experimentally simple but due to the use of relatively high temperature their detailed mechanism might involve different formations of intermediates or precursors. For most of cases decomposition and many side reactions must also be taken into consideration. As an example, Lieber et. al synthesized MgO nanowires with a carbonthermal reduction,[21] where Mg vapour was created *in situ* from the reduction of MgO by carbon, which was carried in a flow reactor to the growth area and oxidized to gain MgO. Hydrogen gas and water instead of carbon could be used as the reducing agent,

and this method could also be extended to other binary oxides such as $A1_20_3$, ZnO, and SnO_2. In all of these syntheses, the formation of metal oxide through a two-step process might help to keep the supersaturation of the system at relatively low levels. [19]

Vapour-liquid-solid method

The vapour-liquid-solid (VLS) process is seen to be the most successful for forming and growing nanowires with single-crystalline structures and in larger quantities than other methods.

A VLS process begins with the dissolution of vapour reactants into small liquid droplets, which acts as a catalyst metal. It is followed by the nucleation and growth of single-crystalline wires or rods. The growth is initiated and controlled by the liquid droplets which sizes remain constant during the entire synthesis of a wire. Both physical and chemical methods can be employed to generate the gaseous reactants needed for nanowire growth. Even no significant derivation has been found in the quality of nanowires synthesized by the different processes. The VLS method has now become a widely used method for generating one dimensional nanostructures from a rich variety of inorganic materials that include semiconductors like Si, Ge and B and oxides like ZnO, MgO and SiO_2. [19]

Template-directed synthesis

In this process the template acts as a scaffold where different materials can be deposited *in situ* and as a result the shape of obtained nanostructures is dictated by the morphology of the template. Two main groups of template assisted growth can occur. In the case where the template is involved only physically, than the necessity arises to selectively dissolve the template using chemical treatment and as a result the resultant nanostructures are obtained. In a case, where the template is chemically consumed as the reaction proceeds, it is possible to directly obtain the nanostructures as a pure product without any post-treatment. Template-directed synthesis provides a simple procedure which allows the complex topology of a template to be duplicated. As a drawback, nanostructures synthesizes using template-directed methods are often polycrystalline and the quantity of structures that can be produced in each run of synthesis is relatively limited. [19]

3.1.3 Applications

Plenty of prototype devices based on NWs were already demonstrated during last few decades including resonance-tunnelling diodes, light emitting diodes, photodetectors, electromechanical devices, piezoresistors, sensors etc. [22-28]. Below in this section some of those will be briefly described.

Field-effect transistor

Silicon NWs have been studied extensively due to the dominance of Si devices in the industry of semiconductors and due to the already developed techniques for growing silicon NWs with doping level and controlled size. In an typical device, the silicon NWs are dispersed into liquid after growth via sonication, then distributed on a doped Si substrate with a oxide layer.

Metal contacts are commonly used in a NW device, contrary to MOSFETs in which the source/drain contacts are formed by degenerated doped Si. In a way a NW field-effect transistor device can be viewed as a Schottky barrier device [29- 32].

Single-electron devices

Zhong et al used the Schottky barriers at the metal/Si contacts as tunnel barriers [32]. The nanowire device can acts as a single-electron transistor at low temperatures, when the charging energy is bigger than the thermal energy [33]. InP NW devices were shown to act like single electron transistors [34]. But the tunnel barriers formed by random defect potentials along the NW, resulting in little control over the device parameters [29,34].

Heterostructure nanowire devices

To obtain high-performance transistors and to measure intrinsic properties of NWs, transparent Ohmic contacts are often demanded. Those contacts can be achieved if heterostructure NWs are band-structure engineered. The Fermi level inside the Si band gap in Ge/Si core/shell NW heterostructures [35], may situate under the Ge valence band and it results in Ohmic contacts. [29]

Waveguides

Plasmonic waveguides made of metal NWs possess significant potential for applications in integrated photonic and electronic devices, where they could help in overcoming fundamental limitations for data transfer rates and bandwidth set in conventional electrical technology [36,37, 38]. When working as a waveguide for plasmon propagation, they have the ability to localize the electromagnetic energy in nanoscale regions which are smaller than the wavelengths of light in the material. [39, 40] The efficiency shown in light manipulation has led to a range of applications, which includes plasmonic routers and multiplexers [41], Bragg mirrors [42], interferometers [43], and electro-optic devices [44, 38].

Nanoelectromechanical switches

Nanoelectromechanical switches work by using electrostatic forces to mechanically deflect a cantilevered element into physical contact with an opposing electrode. Electrostatic forces depend inversely on the square of the gap, making them more effective when devices get smaller. The first nanoelectromechanical-based switches are most likely used where scalability and speed are less critical, but where low power consumption is of key importance. nanoelectromechanical–static-random-access-memory architectures and other hybrid systems have potential to rival conventional CMOS devices in terms of switching speeds while offering reduced power consumption [45]. To build effective and operational switches on the basis of NWs, the fundamental mechanical properties must be known, which yields that mechanical characterization of such nanoswitches is of great importance. [46]

3.2 Experimental techniques employed for mechanical characterization

Many different techniques have been developed for measuring mechanical properties of nanowires. Atomic force microscopes (AFM) or scanning tunnelling microscope based experimental methods have been strong assets for investigation and characterization of mechanical properties of nanowires due to their high force resolution. Salvetat et al [47] performed experiments with an AFM tip. He deflected carbon nanotubes, lying across a hole, and measured their mechanical properties. Comparable methods were used by other workgroups to characterize gold nanowires [48] and polymeric nanowires [49]. Wong et al.

[50] clamped one end of a nanotube and deformed at the other end with AFM tip and calculated the mechanical properties of the nanotube from the displacement.

AFM-based techniques share the high-order resolution which allows the testing of individual nanostructures, but it lacks *in situ* ability. In situ experimental techniques provide direct real-time observation of the dynamic events as they are progressing and they provide qualitative information about the mechanism of motion and deformation. Yu et al [51] conducted tensile tests on multi-walled carbon nanotubes, which were attached to two AFM tips inside a scanning electron microscope (SEM). In situ experimental techniques ensure the efficiency and accuracy of the experimental data, which is most critical in the nanoscale. A popular mechanical testing method is nanoindentation, which has been applied to measure the hardness and elastic modulus of GaN and ZnO nanowires [52]. But the method has some drawbacks as well. The method is affected by the "substrate effect," which comes into play, when nanowires are tested on some substrate. The analysis of dynamic response of a nanowire in an altering current field inside TEM is used, where an oscillating electrostatic field is applied and the nanowire starts to vibrate, when the frequency is equal to the resonant frequency of NW. This technique does not need the wire to be mechanically manipulated, but it does not provide information about mechanical properties of nanowires like fracture strain and toughness and can only be applied in elastic region of nanowire deformation [53, 54]. But the most important indicator, which describes NWs mechanical behaviour, is the Young modulus.

3.2.1 Methods developed for Young modulus measurements

Resonant method

The cylindrical substrate with NWs is mounted directly onto the specimen stage inside a scanning electron microscope (SEM). A homemade nanomanipulator with a sharp tungsten tip [55, 56] was used to approach an individual NW. A frequency-tuneable altering voltage with or without direct current bias was applied across the NW and the countering tip (Fig. 1.). The resonance was directly monitored on the screen of the SEM. Forced resonance occurred at driving frequency $\omega = \omega_o$, while parametric instability occurs at $\omega = 2\omega_0/n$ (n is integer larger than 1) [57]. The extremely small dimensions of nanostructures made it very sensitive to parametric excitation [58-60]. For a NW with random orientation relative to the applied electric field, either parametric resonance or forced resonance may be excited.

Failing to properly distinguish between these two types of resonances would lead to incorrectly determined natural frequency, which may be 2/n (n=1, 2, 3, 4) times the true natural frequency, and results in very large deviation of the modulus, since the Young's modulus is proportional to the square of the frequency.

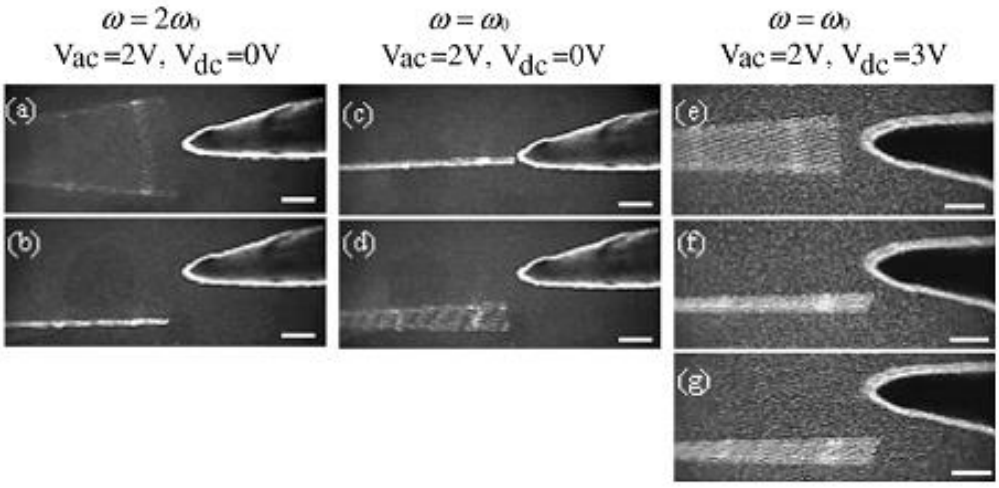

Figure 1. NWs resonance in different electric parameters.

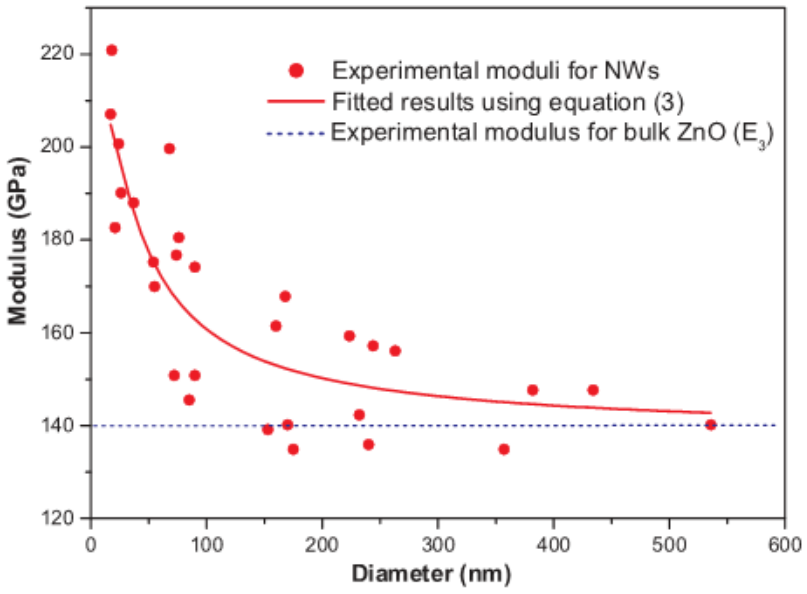

Figure 2. Size dependence of Young modulus.

Size dependence of Young's modulus in [0001] oriented ZnO NWs was experimentally revealed (Fig. 2). The Young modulus of ZnO NWs with diameters smaller than about 120 nm increased dramatically with decreasing diameters, and was significantly higher than that of the larger ones whose modulus was that of bulk ZnO. As a result, they

showed the Young modulus dependence on the radii of NWs, which was in range of 20-550nm, with corresponding Young modulus in range of 135-220 GPa. [61]

Tensile tests

For tensile tests, an AFM chip with two silicon cantilevers on one side was mounted on a sample holder. The ZnO NW was clamped between the nanomanipulator tip and the AFM cantilever, the NW was continuously pushed further than the critical force of buckling. The force and compression data were directly obtained from the images. SEM images were used to obtain the AFM cantilever deflection and due to the fact, that the spring constant of the cantilever is known the load on NW is calculated. During the tensile test, a series of SEM images were taken to measure both force and elongation of the NWs. It can be seen (Figure 3.) that the ends of NW are pinned onto the nanomanipulator tip and AFM cantilever.

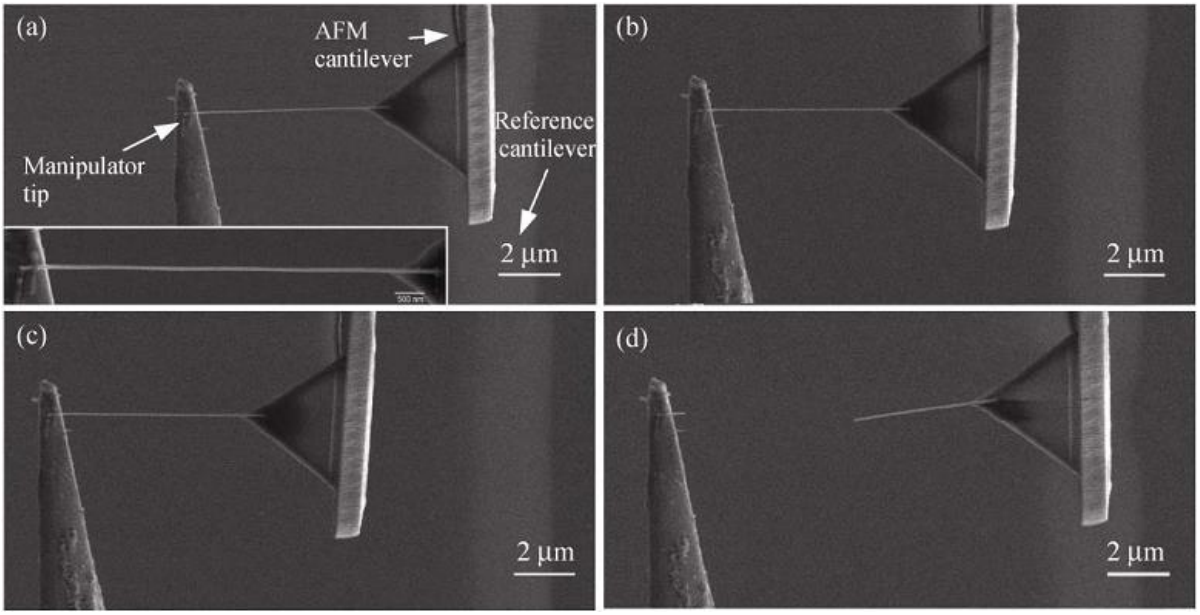

Figure 3. Tensile test of ZnO NW.

Seven ZnO NWs were measured with tensile tests, with diameters ranging from 20-80 nm. The measured Young modulus was in range of 140-170 GPa, where lower values were obtained for NW with smaller radii and it was concluded, that Young modulus depends strongly on the diameter of NW, so the size effect was observed experimentally. [62]

Pure bending method

Manoharan et al [63] synthesized ZnO NWs by the vapour-liquid-solid (VLS) method using gold as a catalyst. The ZnO occurred as clusters and individual NWs were taken with a micromanipulator fitted with a tungsten probe tip. The NW was placed on the edge of a chip of silicon wafer (Figure 4.) perpendicular to the edge using the manipulator.

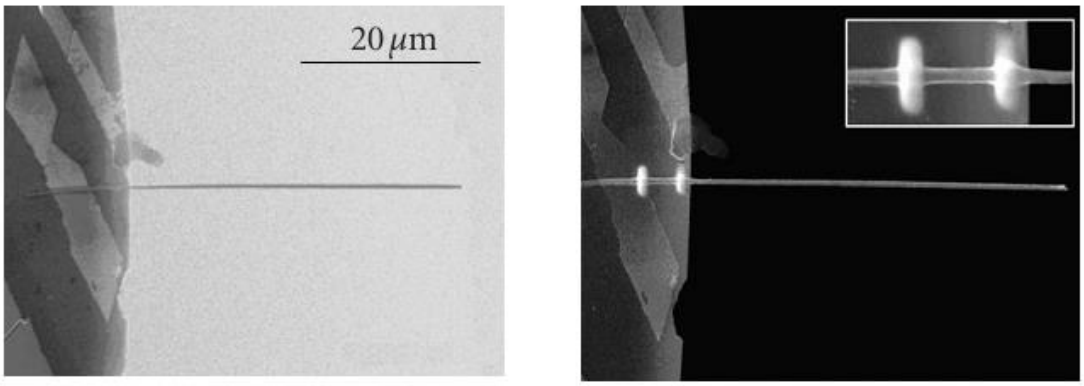

Figure 4. ZnO NWs on Si chip edge.

Cantilever-bending experiments were performed, to measure the Young modulus of the NWs. Bending loads were applied using an AFM cantilever with known spring constant. NWs were bent and corresponding SEM images are taken to evaluate the deflection of NW and AFM cantilever. The following equation is used to estimate the acting stress and strain:

$$\sigma = \frac{32k_{tip}(y_{base}-y_{nw})l}{\pi d^3}, \quad (1)$$

$$\varepsilon = \frac{3y_{nw}d}{2l^2}, \quad (2)$$

where k_{tip} is the stiffness of the AFM cantilever tip, y_{base} is the displacement of the AFM cantilever base, y_{nw} is the displacement of the NW, d is the diameter of the NW, l is length of NW, and the stresses σ and strains ε are the maximum values that occur on the outermost diameter of the NW at the clamped end. Using the deflection values of the AFM cantilever base, NW tip and (Eq. 1.), the normal stress and strain on the NW can be calculated, and a stress-strain diagram is plotted. The slope of the stress-strain curve (linear fit) is Young's modulus of the Nw. NW diameters ranged from 350–750 nm and no dependence of Young modulus on the diameter of the NW was observed. Young modulus was measured for 5 NWs and the results ranged from 35 GPa to 44 GPa. The explanation for the reduction in Young modulus compared to bulk lies in the strong electromechanical coupling in ZnO. Due to its

non-centro-symmetric wurtzite structure and ionic nature of the interatomic bond, internal electric fields are induced in ZnO, when the material is strained [64, 65].

3.2.2 Methods developed for static friction measurements

Friction between a NW and a flat substrate has been studied by means of AFM [66, 67, 68]. It was shown that NWs possess enhanced flexibility compared to bulk [69]. At the same time NW-substrate adhesion and static friction can be high enough to preserve the NW in the bent state. The equilibrium between elastic and friction forces can be utilized to analyse the distributed friction from the known NW bending profile and NW elastic modulus. Such an approach was firstly described by Bordag et al. in [68] and further developed by other authors [66, 67, 70]. The different methods known from literature are discussed in the following section.

Bordag's method

This technique [68] is based on the knowledge that for an ideal elastically deformed wire pinned by adhesion forces to a flat surface and in equilibrium between static friction forces and restoring elastic forces, the most tightly bent regions contain information about the maximal static friction force, that is, about the interfacial lateral force. Experimentally, the NWs are bent in a controlled manner using the tip of an AFM. After the manipulation, the most-bent state can be determined by visual inspection of AFM micrographs (Fig. 5). Assuming bulk values for the Young modulus, the shear stress can be obtained from a straightforward analysis according to the classical theory of elasticity.

A bent wire stores an elastic energy U given by the known formula:

$$U = \frac{EI}{2} \int \kappa(l)^2 dl, \tag{3}$$

where E is the Young modulus, I the area moment of inertia and κ the local radius of curvature. The integration is over the length of the wire. Assuming the NW to be in the most-bent state, it forms a circle and the formula given above transforms into:

$$U = \pi \frac{EI}{R}. \tag{4}$$

Differentiating this expression with respect to the radius and reversing the sign yields the force acting on the whole circumference. Dividing this force by the circumference of the wire gives the force per unit length:

$$F_n^{st} = \frac{EI}{2}\kappa^3 . \tag{5}$$

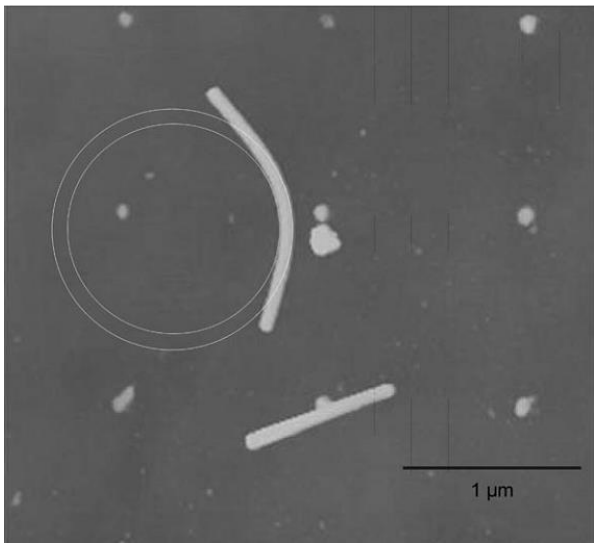

Figure 5. The NW after manipulation. The circles are drawn to determine the inner and outer curvature radii.

Strus' method

Strus [67] described a technique based on high resolution AFM topographical images of carbon nanotubes, which were manipulated into different shapes on a surface to induce local strain. The strain energy distribution of lateral frictional forces acting on curved single-wall carbon nanotubes (SWCNT) as a function of length is calculated. A series of AFM manipulation experiments were presented to demonstrate the capabilities of the strain energy lateral force algorithms developed by Strus [67] to map out the stored flexural strain energy and static friction forces. The carbon nanotube (CNT) profiles were retrieved from AFM images using DataThief, a programme for image analysis.

Strus [67] calculated the lateral friction force from the equilibrium balance of force and moment, which yielded in the following equation for static friction force:

$$F_n^{st} = EI\,\frac{d^2\kappa}{dl^2} . \tag{6}$$

The result of friction force distribution using equation (6) is depicted on Figure 6.

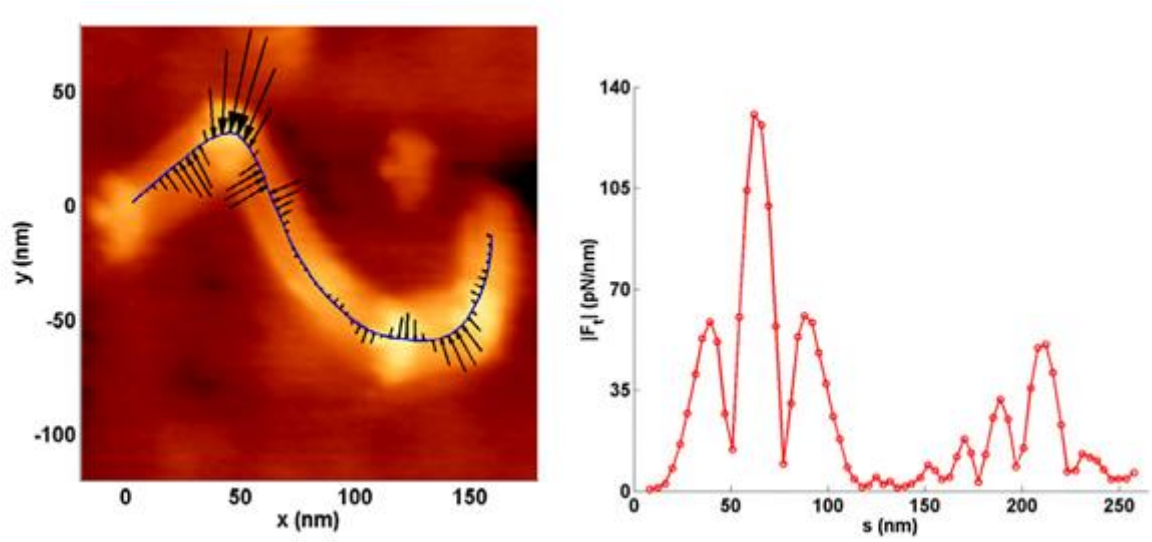

Figure 6. Static friction distribution of bent CNT.

In each manipulation, the AFM tip was dragged across the surface in a 200–300 nm straight line while operating in contact mode with a constant normal force, typically, at least 50 nN. After manipulation, attractive regime amplitude-modulated AFM was used to image the CNTs.

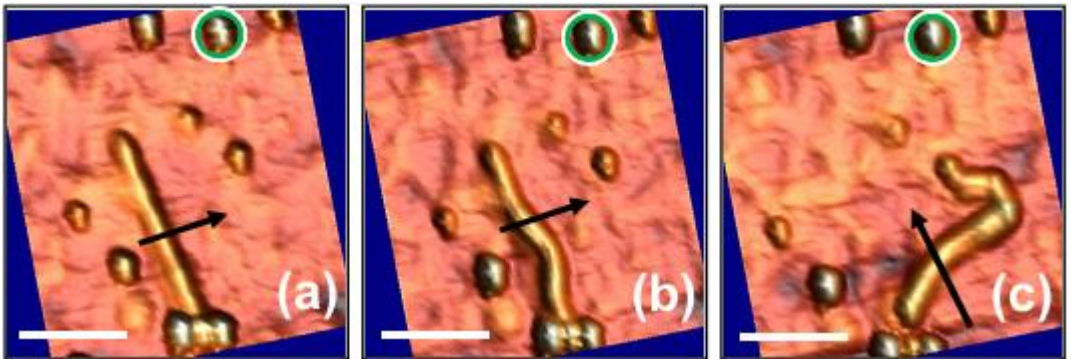

Figure 7. Noncontact AFM images showing a series of manipulations on CNTs.

The SWCNT in Figure 7 was initially straight and then subsequently manipulated into the shapes shown in Figures 7. (a)–(c) leading to a final structure. The arrows in each image represent the direction the AFM tip was dragged across the surface in contact mode, thus deforming the CNT into each subsequent shape. [67]

Stan's method

AFM manipulation was used to bend as-grown Si and fully oxidized Si NWs into a hook or loop shape. In the proposed NW bending method, the in-plane geometry of a bent NW was obtained after each manipulation step by taking the corresponding AFM topographic image. The AFM image was analysed and as a result the local bending stress was calculated which was used to calculate the static friction force distribution (Fig. 8).

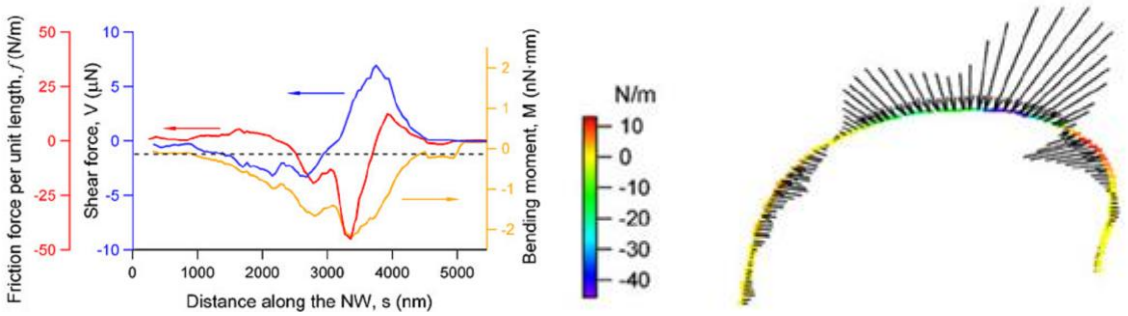

Figure 8. Static friction, shear force and bending moment distribution (left) and visualization of static friction (right).

The coordinates, *x* and *y*, which defined the NW profile in the plane of scan were retrieved from AFM images with help of DataThief. A parabolic fit, $y=Ax^2+Bx+C$, was introduced to the coordinates obtained from the image and the coefficients (A, B, C) were gained which were used to calculate the static friction force along the NW.

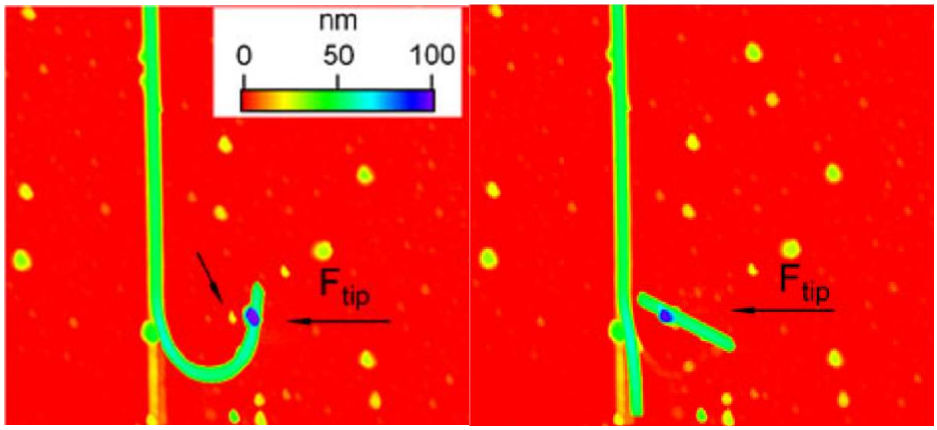

Figure 9. The last bending (left) and failure (right) of Si NW.

The method is similar to Strus' [67] method in terms of the distributed friction force equation, but due to the usage of parabolas the calculated result differs from Strus' result. [66]

4. MATERIALS AND METHODS

4.1 ZnO NWs

ZnO NWs grown using Au nanoparticles as catalyst in the VLS method [71] were chosen for manipulation experiments. NWs obtained by VLS method have shown well-defined geometrical structure, with well-structured facets and proper mechanical properties for manipulation experiments. The NWs obtained ranged in length from 10-20μm and diameter in the range of 60-200nm. The NWs were mechanically transported from the VTM grown substrate by either scraping it with sharp tip or using cleanroom wipes to pick up wires by touching the substrate and moving to silicon surface. During transport NWs were broken into shorter pieces in the range of 1-10μm.

4.2 Experimental set-up

Manipulation experiments were conducted inside a SEM (Tescan VEGA II) using contact AFM cantilever (Nanosensor ATEC-CONT cantilevers C=0.2 N/m) mounted onto a 3-dimensional nanomanipulator (SmarAct SLC-1720-S). Geometry of the cantilever provided tip visibility from the top.

For mechanical characterization of ZnO NWs the home-made force sensor was used. Force sensor was made by gluing the AFM cantilever with a sharp tip to one prong of a commercially available quartz tuning fork (QTF). In experiments QTF is driven electrically on its resonance frequency in self-oscillation mode. Oscillation parameters of such system strongly depend on the forces acting on the tip, which enables to measure the forces involved in manipulations. The signal from the QTF was amplified by lock-in amplifier (SR830, Stanford Research Systems) and recorded through the ADC-DAC card (NI PCI-6036E, National Instruments). The typical values of the driving voltage were 20-50 mV and corresponding tip oscillation amplitude in order of 100 nm. In experiments, tip oscillated parallel to the sample surface (shear mode) and normal to NWs. The force sensitivity of the sensor was calibrated on pre-calibrated AFM cantilevers (FCL, AppNano and CSG11 C=0.03-0.1 N/m, NT-MDT). The tip was electrically connected to the QTF electrode to exclude charging effects. To make the QTF response faster, the Q-factor was reasonably

decreased by putting a small drop of epoxy resin (Ecobond 286, Emerson & Cuming) onto the opposite prong of the QTF.

4.3. Elastic beam theory employed for tribological and mechanical measurements

Let us consider a prismatic NW elastically bent in plane under external lateral forces, which may consist of uniformly distributed or point forces. As a result, the NW is kept in equilibrium due to the balance of intrinsic elastic forces and external forces. In this case the common EBT [72] can be employed to find the equilibrium equations for the NW. They will include the force **F** and momentum **M** of elastic stress defined as integrals by cross-section *S* at any given point *l* along NW axis by components [72]:

$$F_i = \int_S \sigma_{i\gamma} n_\gamma dS\,, \tag{7}$$

$$M_i = \int_S e_{i\alpha\beta} r_\alpha \sigma_{\beta\gamma} n_\gamma dS\,, \tag{8}$$

where $\sigma_{\beta\gamma}$ are components of stress tensor, η_γ the components of normal vector of the elements of cross-section area *dS*, r_α the components of radius vector from the axial point *l* and $e_{i\alpha\beta}$ is the unit anti-symmetric tensor. Both the momentum **M** and elastic force **F** are functions of the coordinate *l* along the axis of the NW.

For a NW at equilibrium, the equations of the full system between force **F** and momentum **M** are as follows:

$$\frac{d\mathbf{F}}{dl} = -\mathbf{f}\,, \tag{9}$$

$$\frac{d\mathbf{M}}{dl} = \mathbf{F} \times \mathbf{t}\,, \tag{10}$$

where **f** is the external distributed force per unit length acting on NW and **t** is the tangent vector of the NW axis.

For the pure bending case of prismatic NWs the following equations were obtained:

$$\mathbf{M} = EI\mathbf{t} \times \frac{d\mathbf{t}}{dl}\,, \tag{11}$$

where *E* is the Young modulus and *I* is the area moment of inertia of the NW. Since the NW deformation in plane, **M** is always directed out of plane and equation (11) can be rewritten as:

$$M = EI\frac{d\varphi}{dl} = EI\kappa, \tag{12}$$

where curvature κ can be defined as $\kappa = d\varphi/dl = 1/R$, where φ is the tangent angle along the NW in point l, R is the local radius of curvature.

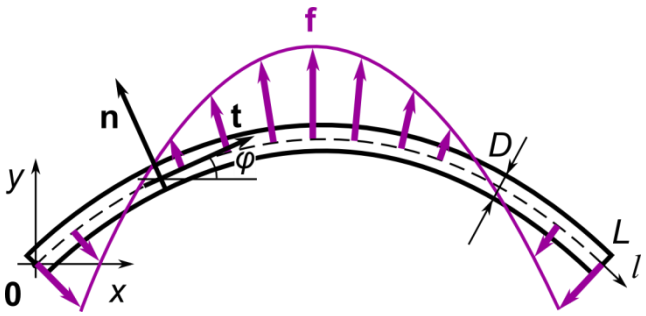

Figure 10. Schematics of a NW of length L and diameter D held in bent state by in-plane distributed lateral force f. Fixed coordinates system $Oxyz$ and local coordinate basis (t,n) along the NW axis l are used. Angle between the tangent vector t and axis Ox is denoted as φ.

Nanowire bent while clamped at one end

Let us consider a NW of length L fixed at one end and loaded by a concentrated force $\mathbf{F}_{\text{load}}$ perpendicular to the initial straight NW line (Figure 10). This problem is classical and described in textbooks (e.g. [73]) through the following equilibrium equation along the NW axis:

$$EI\frac{d^2\varphi}{dl^2} + F_{\text{load}}\cos\varphi = 0. \tag{13}$$

Boundary conditions for the fixed end and for the zero momentum **M** at the other end dictate:

$$\left.\frac{d\varphi}{dl}\right|_{l=L} = 0, \tag{14}$$

$$\left.\varphi\right|_{l=0} = 0. \tag{15}$$

NW profile can be then expressed via elliptic integrals or calculated numerically from the tangent angle $\varphi(l)$ directly from Eq. (13). For the reference, the length of the NW from 0 to the current point as a function of the current tangent angle is:

$$l = \sqrt{\frac{IE}{2F_{\text{load}}}}\int_0^{\varphi}\frac{d\varphi}{\sqrt{\sin\varphi_0 - \sin\varphi}}, \tag{16}$$

where $\varphi_0 = \varphi|_{l=L}$ is the tangent angle at the free end, which correspondingly can be found from Eq. (16) knowing the overall length L through the following equation:

$$L = \sqrt{\frac{IE}{2F_{\text{load}}}} \int_0^{\varphi_0} \frac{d\varphi}{\sqrt{\sin\varphi_0 - \sin\varphi}}. \tag{17}$$

The profile of the NW in Cartesian coordinates can be expressed therefore as:

$$x = \sqrt{\frac{2IE}{F_{\text{load}}}} \left(\sqrt{\sin\varphi_0} - \sqrt{\sin\varphi_0 - \sin\varphi} \right), \tag{18}$$

$$y = \sqrt{\frac{IE}{2F_{\text{load}}}} \int_0^{\varphi} \frac{\sin\varphi \, d\varphi}{\sqrt{\sin\varphi_0 - \sin\varphi}}. \tag{19}$$

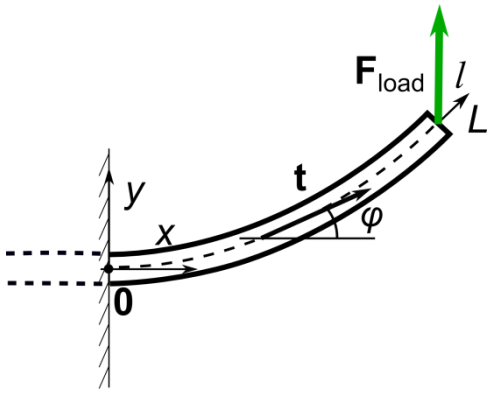

Figure 11. Schematics of NW fixed at one end and loaded at the other end by concentrated force F_{load}.

Nanowire dragged on surface

When a NW is being uniformly dragged at its midpoint without rolling and all parts of the NW have the same constant velocity, the equilibrium equations Eq. (9, 10) are still applicable due to Galileo's principle of relativity. In this case, the profile of the deformed NW is determined by the balance of the external driving tip force, the kinetic friction between the NW and the substrate and the intrinsic elastic forces of the NW. The distributed driving force $\mathbf{F}_{\text{apl-lat}}$ can be modelled via the delta function, and the kinetic friction $\mathbf{q}^{\text{kin}}$ maintains a constant vector opposite to the direction of motion and $\mathbf{F}_{\text{apl-lat}}$ (Fig. 12):

$$\boldsymbol{f} = \boldsymbol{q}^{\text{kin}} + \boldsymbol{F}_{\text{apl-lat}} \cdot \delta\left(l - \frac{L}{2} \right), \tag{20}$$

where $\delta(x)$ is Dirac's delta-function.

The condition of zero total force yields $\mathbf{F}_{\text{apl-lat}}=-\mathbf{q}^{\text{kin}}L$. Zero elastic force and momentum at the free ends of the NW dictate the boundary conditions [73]:

$$\boldsymbol{F}\big|_{l=0} = \boldsymbol{F}\big|_{l=L} = 0, \tag{21}$$

$$\boldsymbol{M}\big|_{l=0} = \boldsymbol{M}\big|_{l=L} = 0. \tag{22}$$

The differential equation of "kinetic" equilibrium of the NW on the interval *(0, L)* directly follows from Eqs. (9-11):

$$IE\frac{d^2\varphi}{dl^2} = -q^{\text{kin}}\left[l - LH\left(l - \frac{L}{2}\right)\right]\cos\varphi, \tag{23}$$

where $H(x)$ is the Heaviside step function. The Eq. (20) can be solved numerically in order to obtain the NW profile. It is easy to see that the solution of Eq. (20) together with the initial condition $\varphi'(0) = 0$ fully complies with the free boundary conditions Eq. (20a,b).

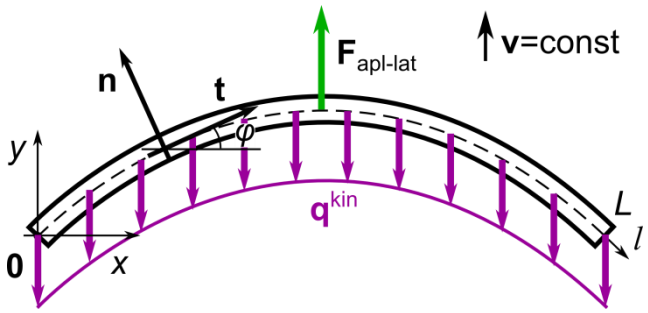

Figure12. Schematics of a NW of length *L* being pushed at the midpoint by concentrated force $F_{\text{apl-lat}}$ and affected by distributed kinetic friction force q^{kin}. Fixed coordinates system *Oxyz* and local coordinate basis (*t*,*n*) along the NW axis *l*. Angle between the tangent vector *t* and axis *Ox* is denoted as φ.

Nanowire equilibrium while lying on surface

In the case when the NW had been preliminarily bent by an actuator, it can be sustained in bent state by static friction forces from the substrate after the removal of the external load. The equations of equilibrium for a purely bent NW affected by distributed static friction force $\mathbf{f}(l)=\mathbf{q}^{\text{st}}(l)$ give (see Fig. 10 and, e.g., [73]):

$$\frac{dF_t}{dl} - \kappa F_n = -q_t^{\text{st}}, \tag{24}$$

$$\frac{dF_n}{dl} + \kappa F_t = -q_n^{\text{st}}, \tag{25}$$

$$EI\frac{d\kappa}{dl} = -F_n, \tag{26}$$

where F_t and F_n are the projections of elastic force **F**, q_t^{st} and q_n^{st} are the projections of $\mathbf{q}^{st}$ to the local coordinates (**t**, **n**). The complete set of boundary conditions Eqs. (21-22) applied to the system Eqs. (24-26) yields:

$$\kappa|_{l=0} = \kappa|_{l=L} = 0, \tag{27}$$

$$\left.\frac{d\kappa}{dl}\right|_{l=0} = \left.\frac{d\kappa}{dl}\right|_{l=L} = 0. \tag{28}$$

The tangential component of the friction $q_t^{st} = 0$ will be neglected, thus making the system of Eqs. (24-26) complete and yielding:

$$F_t = -EI\int_0^l \kappa\frac{d\kappa}{dl}dl = -EI\frac{\kappa^2}{2} \tag{29}$$

$$q_n^{st} = EI\left(\frac{d^2\kappa}{dl^2} + \frac{\kappa^3}{2}\right), \tag{30}$$

which solves the system together with the initial condition $F_t|_{l=0} = 0$. The absence of a tangential friction component does not lead to the vanishing of F_t which is then fully "driven" by the normal component F_n and necessary for exact NW equilibrium.

It is important to note that the assumption $q_t^{st} = 0$ was dictated by an intuitive consideration that the direction of $\mathbf{q}^{st}$ should be close to the direction at which the NW tends to unbend. This "unbending" direction correspondingly lies close to normal to the NW's line. Formally it means that the integral contribution of q_t^{st} along the length of the NW is much smaller than that of q_n^{st}. Moreover, the tangential component of force does not contribute to bending in the framework of the given model and is considered to be a small effect of higher order.

5. RESULTS AND DISCUSSION

In this part the experimental details of nanomanipulation experiments are described. First, results of Young modulus measurements are presented. Secondly, kinetic friction measurement experiments are demonstrated with corresponding results. Finally, the static friction measurements are presented along with comparison of different methods found in literature.

5.1 Young modulus measurements

Si wafers used for Young modulus measurements contained 1 μm deep and 2 × 2 μm wide trenches (Fig. 13b) cut by focused ion beam (Helios NanoLab, *FEI*). Experiment started with finding NW that had appropriate parameters (uniform thickness, sufficient length) and situated in the close proximity of the patterned area. The selected NW was moved then by the AFM tip toward nearest trench and positioned over its edge so that one end of the NW was suspended over the trench while another end was fixed to the substrate surface by the adhesion force. Measurement procedure consisted in bending of the NW suspended part by the AFM tip in direction parallel to the trench wall (Fig. 13). The QTF oscillation amplitude signal (which directly correlates with the applied force) and SEM images were recorded simultaneously during the measurements. For the calculation of Young modulus the NW profile from the SEM image was numerically fitted to the curve given by the equation of equilibrium for a bent elastic beam and the value of Young modulus was extracted.

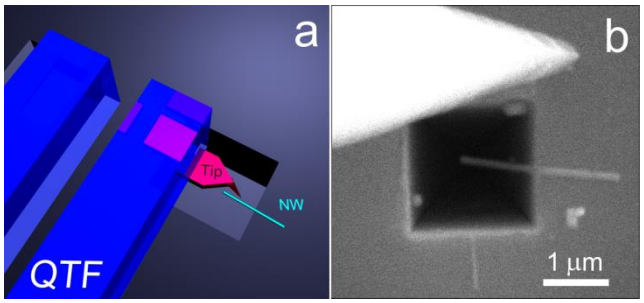

Figure 13. Schematics of experiment. (a) QTF with the glued AFM tip contacts a NW suspended over a trench on the silicon sample; Corresponding SEM image of the AFM tip, NW and trenches can be seen (b).

The typical force curve and the corresponding SEM images are presented in Fig. 14. The averaged value of Young's modulus for 13 different NWs was found to be 58±34 GPa. The mean value is in good agreement with other works performed on ZnO NWs. Manoharan *et al*. found 40 GPa for a NW with the diameter of 200–750 nm [63] and Song *et al*. found 29 GPa for a NW with the diameter of 45 nm [74]. Significant variation in magnitudes of Young's modulus from 22 to 117 GPa in the measured set of NWs clearly evidences the importance of gathering the Young's modulus for each NW individually.

The proposed method opens a route to measure Young's modulus of rather short NWs with lengths of a few microns. In experiments, the length of the suspended part of NW was about 1-2 μm in contrast to at least a few tens of μm in other works dealing with NW bending [75,54].

Another advantage of the method is that there is no need to worry about fastening of the NW to the substrate. The static friction force between the NW and the substrate was high enough to keep the adhered part of the NW in place as it was visible in SEM. It would make sense to assume that in such hard contact any "floating" deformations were not possible. In some cases when the force was sufficiently high, sudden slips of NW were observed. Then the before-slip interval was used for the analysis. It is also worth noting that breaking of NW was never observed in the bending experiments, even at large bending angles ($\theta \approx 60°$).

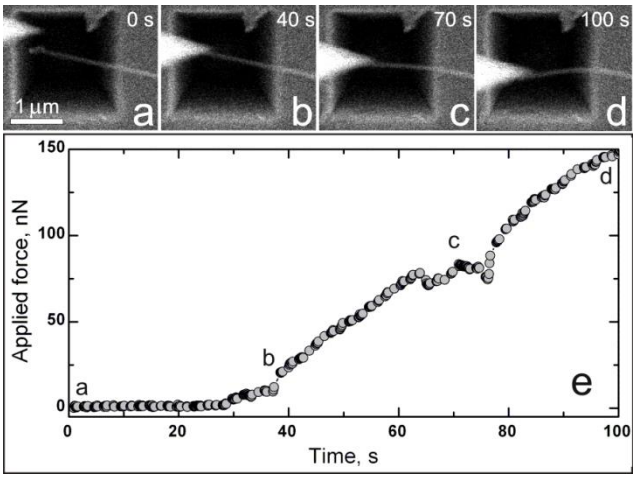

Figure 14. SEM images of the suspended NW being pushed by the tip and the corresponding force-time curve. The tip approaches the NW, the arrow indicates the direction of tip movement (a); The NW is slightly bent (b); Maximal bending of NW and the corresponding schematics of the NW loading. The NW has come off the tip and the force has dropped to zero (d). The calculated Young's modulus is E=104 GPa.

5.2 Kinetic friction measurements

For the kinetic friction measurements a NW was translated along the substrate surface by pushing it at its midpoint with AFM tip. During dragging the NW bent into an arc of a certain curvature that is determined by balance of NW-substrate kinetic friction and elastic forces inside the NW. The profile of the NW remained constant during translation and was used to determine the kinetic friction force distributed along the NW (Fig. 15).

The determination of the kinetic friction was problematic for the relatively low aspect ratio NWs (shorter than about 3 μm for 100 nm thickness) due to the large radius of the curvature during the translation. Thus, longer NWs were preferable.

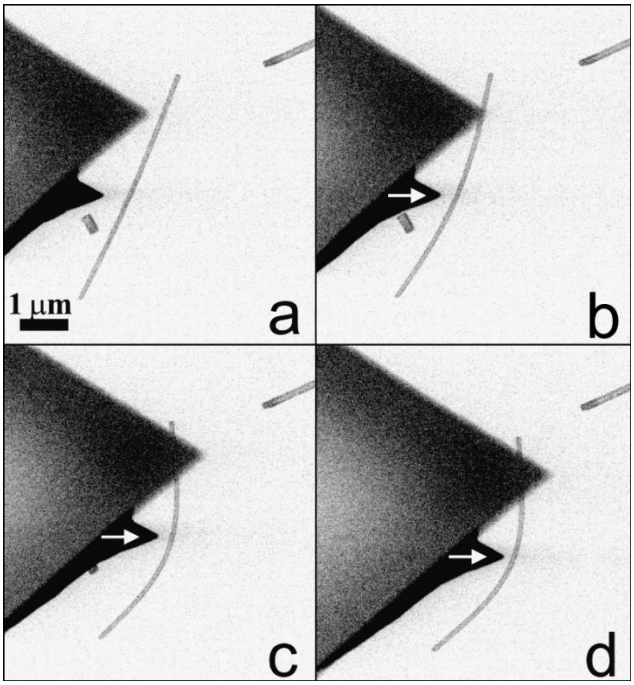

Figure 15. SEM images of the ZnO NW shape profile during the NW dragging. The AFM tip contacts the intact NW, the arrow indicates the direction of tip movement (a); Partially displaced NW (b); Completely displaced NW (c); Final characteristic shape(d).

For calculation of the distributed kinetic friction force the EBT was applied. NW length *L*, diameter *D* and profile during manipulation were obtained from the SEM images. Actual values of Young moduli measured individually for each NW were used for the calculation.

The measurements were performed on eight NWs with different diameters on Si/SiO_2 substrate. The average value of the kinetic friction force ranged from 0.03-0.7nN/nm. It was shown, that kinetic friction tended to grow, when NW diameter increased. The average value

of the interfacial shear stress is q_{kin}=3.2 MPa and 2.1 MPa [69]. These results are in a good agreement with Manoharan *et al.* who obtained 1 MPa for the interfacial shear stress for ZnO 30-40 μm long NWs with 200 nm diameters parallel to the NW axis dragging [76].

5.3 Static friction measurement with different analytical methods

Single NW on silicon surface was manipulated by the following procedure. The substrate with deposited NWs was inspected in SEM and single NW of appropriate aspect ratio in the range of 30-60 was selected. Those NWs can be bent into complex shapes more easily. For lower aspect ratios the elastic forces in bent NW tend to overcome static friction and only common shapes, like arc-shapes can be observed. Proper NW was chosen and gradually bent in plane with the AFM tip. After retraction of the tip the residual bent shape of the NW was determined by the balance between elastic and interfacial forces. The procedure was repeated many times and different shapes of NWs were obtained.

A single S-shaped NW with appropriate aspect ratio was chosen (Fig. 16) and different methods for calculation of distributed friction force were applied and compared.

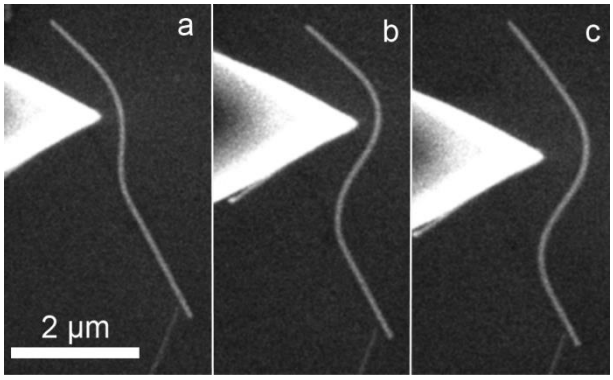

Figure16. Continuous set of SEM images of ZnO NW bent into S-shape by AFM tip and. The NW diameter is 90nm and length is 5.5μm.

Firstly it is necessary to know the exact geometry, size and elastic modulus of the NWs for the application of EBT and determination of distributed friction force in all considered methods. Those properties strongly influence the interfacial forces acting between the surface and the NW and thus affect the mechanical behaviour of NWs. The cross-section of ZnO NWs used in experiment is assumed to be hexagonal [77]. Young's modulus of 58GPa was used, as measured for the same type of ZnO NWs in earlier work [78].

Second step is skeletonization, i.e. extracting the centreline and subsequently the local curvature distribution function. Different authors used different skeletonization procedures. Stan [66] and Strus [67] both used the software DataThief, although the final skeleton for friction analysis was obtained slightly differently. Strus [67] used the raw DataThief data and smoothened it with three- and five-point running mean average filters. Stan provided no information about smoothening and therefore the assumption was made that the raw skeleton was used. Stan applied parabola-fits, where a parabola in the form $y=Ax^2+Bx+C$ was fitted at each point along the NW skeleton comprising six adjacent points (three at each side).

The skeletonization proposed by Dorogin et al. in [69] is distinctive in the usage of specially defined polynomials for curvature distribution. It enabled to comply with the boundary conditions of the free ends of the NW already at the stage of skeletonization. Another advantage is direct fitting and interpolation of the centreline, without necessity for additional filtering.

Bordag in his original paper [68] did not use any skeletonization algorithm. Instead a circle was fitted to the image of the NW to find the single value of radius of curvature in the most bent part of the NW for determination of maximum value of static friction. In the current paper curvature function based on Dorogin's method were used for Bordag's static friction calculation to obtain friction force values not only in the most bent state, but at each point of the NW.

At the third (final) step the static friction force distribution, the elastic energy distribution and the total elastic energy can be calculated if the curvature distribution is known. The analytical expressions for the friction distribution are summarized in Table 1. Bordag [68] on the basis of the fact that an elastically bent beam stores a certain amount of elastic energy extracted the restoring force of circularly bent beam and identified it as the static friction force.

Strus [67] and Stan [66] calculated the friction force from the equilibrium equations of elastic beam without taking the boundary conditions into account. Moreover, as can be seen from the Strus' expression, only the 3rd derivative term is present. Stan had used the same solution for the friction distribution, but expressed in the terms of parabolic coefficients A and B. Due to the algebraic mistake found in [66] the expression was corrected and used henceforth.

Dorogin [69] had employed the equilibrium equations likewise, but with a different result. The 2nd term proportional to the curvature had emerged.

Table 1. Analytical expressions and calculated values of static friction distribution between the complexly bent NW and substrate.

Authors	Static friction between the NW and substrate		
	Analytical expression	Average value, nN/nm	Maximal value, nN/nm
Bordag et al. [66](*)	$F_n^{st} = \frac{EI}{2}\kappa^3$	0.024	0.1
Strus et al. [67]	$F_n^{st} = EI\frac{d^2\kappa}{dl^2}$	0.21	0.49
Stan et al. [66] (**)	$F_n^{st} = -EI\frac{24A^3(16A^2x^2+16ABx+4B^2-1)}{(4A^2x^2+4ABx+B^2+1)^{\frac{9}{2}}}$	0.19	1.4
Dorogin et al. [69]	$F_n^{st} = EI(\frac{d^2\kappa}{dl^2}+\frac{\kappa^3}{2})$	0.20	0.38

(*)modified Bordag using Dorogin's skeleton as a basis

(**) x is the coordinate in the plane of the SEM image.

Let us now consider all described methods in application to the S-shaped NW (see Fig. 2a). The numerical results for the average and maximum static friction per unit length are presented in Table 1 for all the methods. The diagram with static friction distributions along the NW for all the methods is depicted in Fig. 18, whereas Fig. 17 contains friction and elastic energy distributions for Dorogin's method only.

From Table 1, it is evident that the method proposed by Bordag [68] underestimates the friction force. Stan's method also has certain drawbacks. The centreline acquired from the DataThief may contain local disturbances if the original image is not smooth enough. Therefore, Stan's result exposed to high frequency artefacts arising from higher order derivatives used to calculate static friction and therefore is more sensitive to small disturbances in the curvature of the NW. Due to the fact that Strus used averaging filters the obtained static friction distribution is relatively smooth compared to the result obtained by Stan.

Finally, the methods by Bordag, Strus and Stan neglect the role of free ends of NWs. In present paper the skeletonization part was developed further to enable managing and extraction static friction from more complex shapes. Free ends of NW are effectively accounted preventing information lost during processing. The results of the refined Dorogin's algorithm applied to S-shaped ZnO NW are shown in Fig. 17, where the arrows indicate the direction and amplitude of the normal component of static friction.

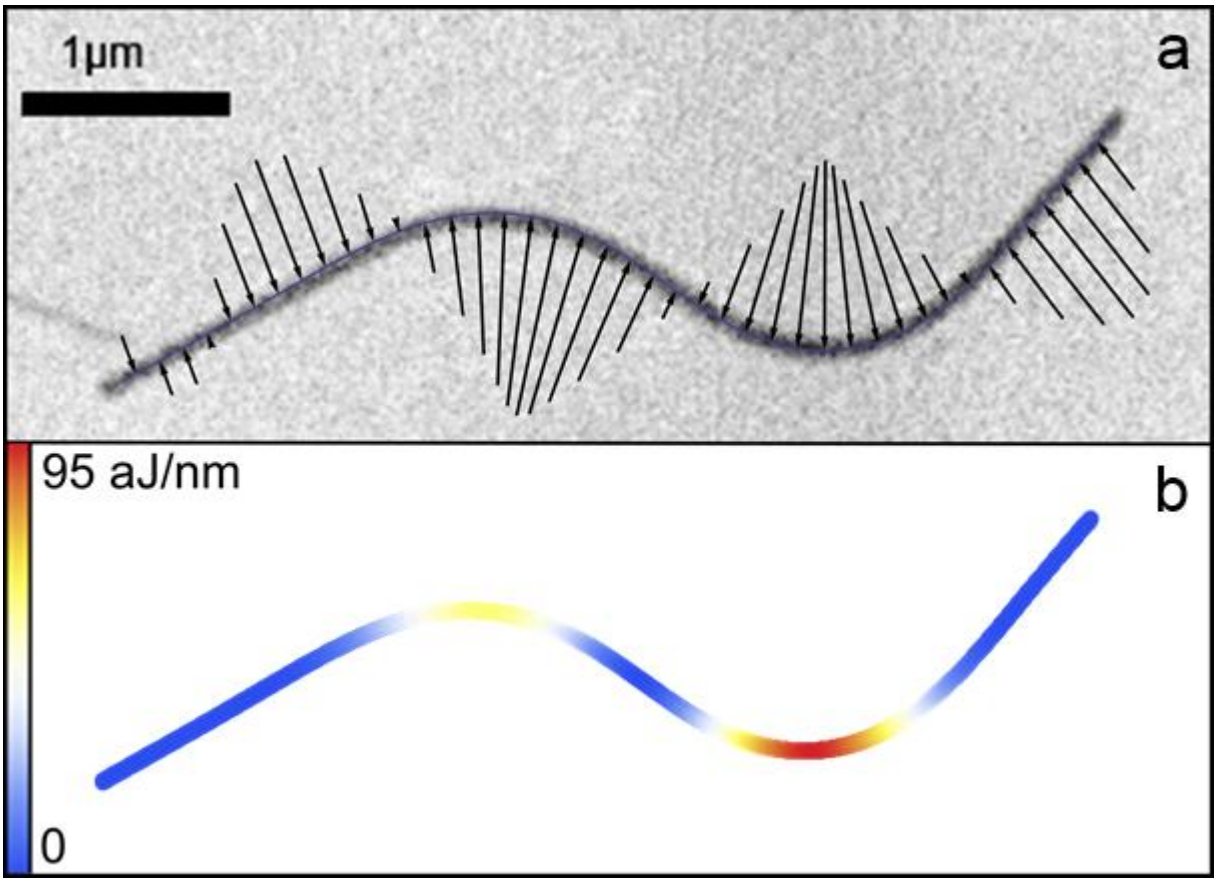

Figure17. Static friction (a). Elastic energy (b). The total calculated elastic energy stored in the NW is 0.14pJ.

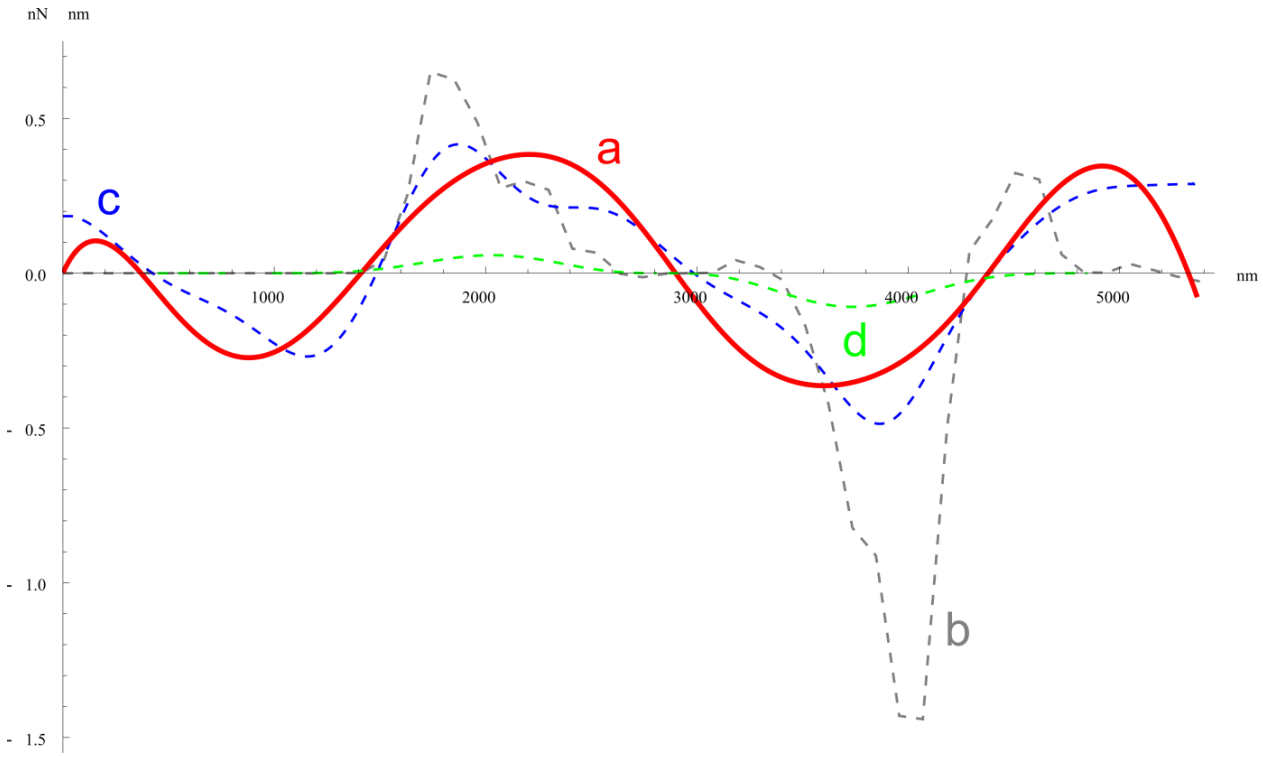

Figure 18. Calculated static friction force distribution along the selected N by four different methods: Dorogin's (a), Stan's (b), Strus' (c), Bordag's (d).

Limitations of the elastic beam model

ZnO NW is a single crystalline material and should possess anisotropy of elastic properties. On the other hand, investigations revealed presence of various defects in NWs grown using VTM [79]. Both facts lead to significant variations in NW's elastic moduli. In fact the measured Young modulus is averaged characteristic related to certain kind of elastic deformation and it may change e.g. if NW has rolled to another contact facet.

Deformation of NW during the manipulation experiments is actually more complicated than purely bent strain assumed by the simple EBT. This is connected with points of application of external forces (distributed friction and tip's concentrated forces) and torques produced by them. As a result of forces applied at NW's sidewalls, direction of the momentum **M** deviates from *Oz* and NW is torqued. Torsion of NW is not considered in the model and, consequently, real magnitude of external force can be higher because the torsional component is neglected.

It is also important to note that no plastic deformation was observed during the bending experiments. Bent NWs released from external forces have relaxed to restore straight profile

Cross section, substrate and contact area

Geometry of NW and particularly cross section require special attention in nanomanipulation experiments, because they determine the area momentum of inertia *I* and NW-substrate contact area and strongly influence on flexibility of the NW. Uncertainty of these parameters can introduce significant scattering in experimentally obtained friction data.

On the contrary to "dry" macroscopic friction, nanoscale friction is controlled by intermolecular van der Waals forces and extensively depends on the contact area. Moreover, even small surface defects ("bumps") may introduce large difference in friction due to rapid decay of van der Waals forces.

Scattering in magnitudes of friction force is sometimes explained by presence of contamination layer in contact area which prevents easy sliding (low friction) that would take place in the case of clean surfaces [80]. Nevertheless, a broad experience in manipulation of ZnO NWs allows to propose rather opposite explanation of scattering in experiments. NWs with visible surface defects or contaminated have demonstrated low friction versus NWs of perfect shape and visibly ideal surface. Sometimes "perfect" NWs were adhered to the substrate so strongly that it was not possible to move them by means of the manipulation setup.

Real-time visual guidance is the technique necessary for correct estimation of the geometry of NW and consequently the contact area. In the most of cases in experiments it was possible to clarify and filter out belt-like and other irregular shaped NWs. However, resolution of the SEM used in experiments did not enable to clearly identify the cross section of NW in some cases. Therefore high resolution microscopy is of critical importance to increase the quality of data analysis.

Other peculiarities

Measurements of Young modulus using QTF-based force sensor involve calibration procedure. The calibration implies that interaction between the sensor and measured sample leads to the same amplitude-force dependence as in case of the reference sample, i.e. calibration curve is invariant. The reference and measured samples are essentially different and the exact conformity of calibration curves would need a special investigation.

Due to high scattering of Young modulus, it would be better to perform deformation-based methods of friction force measurements described in the present paper pairwise with

measurements of Young. Experimentally this is not always possible for each particular NW or might be time-consuming.

Frame rate of SEM observations make it possible to control the state of the system within the timescale of human's responsiveness. Although, characteristic times of NW systems are several orders smaller. The motion seen as smooth translational might be actually stepped movement. In considering measurements of kinetic friction, NW is assumed to be uniformly moving. The actual NW dynamics is a slip-stick motion, which is practically impossible to observe directly. This would mean that during most of time NW is statically adhered and moves only short periods of time. But one can claim that in spite, during the short slip periods the NW reaches equilibrium with the external pushing force, and the bending profile is determined by exactly kinetic friction force. If the NW was bent "weaker" (straighter) than the equilibrium requires, the NW would be deformed further by the tip. If the NW was bent "stronger" than necessary, the NW would relax (become weaker deformed) during the slip. Then static friction only conserves the current bending profile until the next slip. However, the general definition of kinetic friction does not consider underlying mechanics, and is fundamentally macroscopic.

SUMMARY

Due to small dimensions and high aspect ratio NWs have shown to possess fundamentally different properties from its bulk counterparts. The need to have knowledge about real properties of such nanostructures has risen not only due to fundamental aspects but because of miniaturization of electromechanical systems and devices. While being widely used in applications, mechanical and tribological properties of NWs are still poorly studied.

In the framework of the thesis new more accurate methods for characterising tribological and mechanical properties of NWs were proposed and demonstrated experimentally on ZnO NWs on a flat Si surface.

First of all, Young modulus of ZnO NWs was measured by bending half-suspended NW and registering the applied force by home-made force sensor. The EBT based model was implemented for analysis of experimentally obtained force-distance data. For 13 measured NWs the calculated values of Young modulus ranged from 22 to 117 GPa with average value of 58±34 GPa. The results were in a good agreement with other works performed on ZnO NWs.

In order to measure the kinetic friction between ZnO NWs and Si wafer, a NW was dragged from its midpoint and its bending profile was registered. Then the EBT based model enabled to calculate the distributed kinetic friction force acting by numerical fitting. The resulting values for kinetic friction ranged from 0.1-0.3 nN/nm with median value of 0.25nN/nm. The average value of the interfacial shear stress was q_{kin}=3.2 MPa.

Finally, distributed static friction for elastically bent NW was extracted from experimental data. Elastic flexibility of NW is much greater than for bulk materials enabling to bend it into complex shapes that can be preserved by strong adhesion and friction forces even after removal of the manipulator tip. In such case, the analysis of equilibrium of the bent NW provided information about NW-substrate distributed static friction force. Although a number of methods for the analysis had been proposed by different authors, they all leave a field for discussion concerning their limitations and range of errors. The main drawbacks of those methods had rooted in physical equilibrium equations and pre-processing procedures. Due to that, for complexly bent NWs the divergence in friction force could reach an order of magnitude. That evidenced the need for usage of accurate modelling of NW bending profile in complex systems. The refined EBT based method with optimized polynomials exhibited

higher level of accuracy due to the boundary conditions incorporated at the pre-processing stage and full complying of the elastic equilibrium equations.

One more noteworthy advantage of the described methods is a possibility to be applied for various one dimensional nanostructures with practically no limitation on the material used.

Author's contribution

The research presented in the thesis was made in a team work. However, the author participated in the study from its very beginning to the end and contributed to all its main stages. In particular:

- Author participated in development of experimental equipment and prepared drawings of essential parts of the manipulation set-up;
- Author prepared several QTF-based force sensors;
- Author participated in and performed individually manipulations experiments inside scanning electron microscope;
- Author complemented the calculation algorithm and software script for Young modulus measurement based on fitting the experimental bending profile of a NW;
- Author participated in data analysis and performed calculations of Young modulus of NWs;
- Author is implemented three methods described in literature for analysis of static friction forces in elastically bent NWs on a flat surface;
- Author elaborated an improved algorithm for analysis of static friction forces in elastically bent NWs on a flat surface;
- Author applied and compared known methods along with his original method for extraction of distributed static friction from experimental data for elastically bent ZnO NWs on a silicon wafer.

SUMMARY IN ESTONIAN

ZnO nanotraatide mehhaaniline ja triboloogiline karakteriseerimine

Mikk Antsov

Kokkuvõte

Uurimistöö käsitleb tänapäeva materjaliteaduse ja füüsika üht omapärasemat uurimisvaldkonda, kus nanotraatidest koosnevate süsteemide omadused sõltuvad otseselt vastava süsteemi suurusest, mis on vägagi aktuaalne nanoskaalas asuvate süsteemide juures, kus pindala/ruumala suhe on kordades suurem kui makroskoopilstes süsteemides.

Käesoleva magistritöö raames arendati välja uued, täpsemad meetodid nanotraatide mehhaaniliste ja triboloogiliste omaduste karakteriseerimiseks, nii eksperimentaalselt kui ka teoreetiliselt. Meetodite rakendatavust demonstreeriti ZnO nanotraatide manipuleerimiskatsetes tasasel räni pinnal ja katsetulemuste teoreetilises analüüsis. Katseid teostati skaneerivas elektronmikroskoobis, mis võimaldas jälgida otseselt nanotraatite käitumise iseärasusi mõjustamisel aatomijõu mikroskoobi teravikuga või jõusensoriga.

Mehaaniliste omaduste määramiseks manipuleeriti ZnO nanotraate pooleldi-rippudes üle räni pinnal asuvate kanalite ning mõõdeti nanotraadi mehaanilist reaktsiooni jõusensori poolt avaldatava mõju vastu. Mehaaniliste reageeringute mõõtmistulemusi kombineeriti elastsete varraste teooriaga, mille põhjal arvutati üksikute ZnO nanotraatide Youngi moodulid. Arvutatud Youngi mooduli väärtused jäid 22-117 GPa vahemikku.

ZnO nanotraate mõjustati aatomijõu mikroskoobi teravikuga (ilma jõusensorita) räni pinnal, paigutades positsioneeriv teravik traadi keskpunkti ning lohistati mööda pinda . Teatud hetkel vaadeldi nanotraadi profiili tasakaalustumist, mis oli tingitud elastsus- ja hõõrdejõudude vastasmõjust. Vastavast nanotraadi profiilist oli võimalik elastsete varraste teooriat rakendades arvutada kineetilise hõõrdejõu väärtused ja jaotus piki nanotraati. ZnO jaoks jäid mõõdetud kineetilise hõõrdejõu keskmised väärtused 0.03-0.7nN/nm vahemikku.

Nanotraatide erinevate tasakaaluliste profiilide analüüsiks arendati välja uudne täiustatud mudel, mis võimaldab elastsete varraste teooria raames viia läbi arvutusi staatilise hõõrdejõu jaotuse määramiseks. Originaalset metoodikat võrreldi otseselt juba varasemalt teada olevate mudelitega ning näidati, et sõltuvalt mudeli valikust võivad tulemused hõõrdejõu jaotustes erineda suurusjärkude võrra. Erinevate meetoditega arvutatud hõõrdejõu keskmised väärtused jäid vahemikku 0.1-0.49nN/nm.

Acknowledgments

I would like to thank my supervisors, Dr. Leonid Dorogin and Dr. Sergei Vlassov, also my colleagues Dr. Boris Polyakov, Dr. Rünno Lõhmus, Dr. Ilmar Kink and Dr. Ants Lõhmus for their support and help in accomplishing the interesting research for the thesis in the University of Tartu.

This work was supported by the Estonian Science Foundation (grant JD162), ESF FANAS program ‘‘Nanoparma’’, and European Union through the European Regional Development Fund (Centre of Excellence ‘‘Mesosystems: Theory and Applications’’, TK114). The work was also partly supported by ETF grants 8420, 9007, Estonian Nanotechnology Competence Centre (EU29996), ERDF ‘‘TRIBOFILM’’3.2.1101.12-0028, ‘‘IRGLASS’’ 3.2.1101.12-0027 and ‘‘Nano-Com’’ 3.2.1101.12-0010.

REFERENCES

[1] B. Wu, A. Heidelberg, and J. J. Boland, "Mechanical properties of ultrahigh-strength gold nanowires", Nat. Mater. 4, 525-529 (2005).
[2] M. Hocevar, G. Immink, M. Verheijen, N. Akopian, V. Zwiller, L. Kouwenhoven, and E. Bakkers , "Growth and optical properties of axial hybrid III–V/silicon nanowires", Nat. Commun. 3 (2012).
[3] J. Hu, M. Ouyang, P. Yang, and C. M. Lieber, "Controlled growth and electrical properties of heterojunctions of carbon nanotubes and silicon nanowires", Nature 399, 48-51 (1999).
[4] M. Fernandez-Regulez, M. Sansa, M. Serra-Garcia, E. Gil-Santos, J. Tamayo, F. Perez-Murano, and A. S. Paulo, "Horizontally patterned Si nanowire growth for nanomechanical devices", Nanotechnol 24, 095303 (2013).
[5] A. M. Ionescu, "Electronic devices: Nanowire transistors made easy", Nat. Nanotechnol. 5, 178-179, (2010).
[6] Z. L. Wang, "Piezopotential gated nanowire devices: Piezotronics and piezo-phototronics", Nano Today , 5, 540-552 (2010).
[7] P. X. Gao, J. H. Song, J. Liu, and Z. L. Wang, "Nanowire Nanogenerators on Plastic Substrates as Flexible Power Source" Adv. Mater. 19, 67 (2007).
[8] H. He Jr., C. L. Hsin, J. Liu, L. J. Chen, and Z. L. Wang, "Piezoelectric Gated Diode of a Single ZnO Nanowire", Adv. Mater. 19, 781 (2007).
[9] S. S. Kwon, W. K. Hong, G. Jo, J. Maeng, T. W. Kim, S. Song, and T. Lee, "Piezoelectric effect on the electronic transport characteristics of ZnO nanowire field-effect transistors on bent flexible substrates", Adv. Mater. 20, 4557 (2008).
[10] Y. Qin, X. D. Wang and Z. L. Wang, "Microfiber-Nanowire Hybrid Structure for Energy Scavenging", Nature 451, 809-813 (2008).
[11] X. Han, G. Jing, X. Zhang, R. Ma, X. Song, J. Xu, Zh. Liao, N. Wang and D. Yu, "Bending-Induced Conductance Increase in Individual Semiconductor Nanowires and Nanobelts", Nano Res. 2, 553 (2009).
[12] G. Conache, A. Ribayrol, L. E. Fröberg, M. T. Borgström, L. Samuelson, L. Montelius, H. Pettersson, and S. M. Gray, "Bias-controlled friction of InAs nanowires on a silicon nitride layer studied by atomic force microscopy", Phys. Rev. B 82, 035403 (2010).
[13] Y. Peng, I. Luxmoore, M. D. Forster, A. G. Cullis, and B. J. Inkson, "Nanomanipulation and electrical behaviour of a single gold nanowire using in-situ SEM-FIB-nanomanipulators" J. Phys. Conf. Ser. 126, 012031 (2008).
[14] S. K. Lee, H. J. Choi, P. Pauzauskie, P. Yang, N. K. Cho, H.-D. Park, E. K. Suh, K. Y. Lim and H. J. Lee, "Gallium nitride nanowires with a metal initiated metal-organic chemical vapor deposition (MOCVD) approach", *Phys. Status Solidi B* 241, 2775–2778 (2004).
[15] Z. L. Wang, R. P. Gao, P. Poncharal, W. A. de Heer, Z. R. Dai and Z. W. Pan, "Mechanical and electrostatic properties of carbon nanotubes and nanowires", *Mater. Sci. Eng. C* 16 ,3–10 (2001).
[16] M. S. Dresselhaus, Y.-M. Lin, O. Rabin, M. R. Black and G. Dresselhaus, *Springer Handbook of Nanotechnology*, edited by Bharat Bhushan, pp. 99-145 (2004).
[17] Z. Zhang, M. Qiu, U. Andersson, L. Tong, "Subwavelenght-diameter silica wire for light in-coupling to silicon-based waveguide", *Chin. Opt. Lett*. 5 577-579 (2007).
[18] R. Agrawal, B. Peng, H. D. Espinosa, "Experimental-Computational Investigation of ZnO nanowires Strength and Fracture", Nano Lett. 9, 4177-4183 (2009).
[19] Y. Xia, „One-Dimensional Nanostructures: Synthesis, Characterization, and Applications", Adv. Mater. 15, 353–389 (2003).

[20] Y. Zhang, N. Wang, S. Gao, R. He, S. Miao, J. Liu, J. Zhu, X. Zhang, „A Simple Method To Synthesize Nanowires“, Chem. Mater. 14, 3564 (2002).
[21] P. Yang, C. M. Lieber, „Nanostructured high-temperature superconductors: creation of strong-pinning columnar defects in nanorod/superconductor composites“, J. Mater. Res. 12, 2981 (1997).
[22] A. Kolmakov, Y. Zhang, G. Cheng, M. Moskovits, "Detection of CO and O_2 Using Tin Oxide Nanowire Sensors", *Adv. Mater*. 15 997-1000 (2003).
[23] L. Samuelson, M. Bjork, K. Deppert, M. Larsson, B. Ohlsson, N. Panev, A. Persson, N. Skold, C. Thelander, L. Wallenberg, "Semiconductor nanowires for novel one-dimensional devices", *Physica E* 21 560-567 (2004).
[24] C. Soci, A. Zhang, B. Xiang, S. Dayeh, D. Aplin, J. Park, X. Bao, Y. H. Lo, D. Wang, "ZnO Nanowire UV Photodetectors with High Internal Gain" *Nano Lett*. **7,** 1003-1009 (2007).
[25] M. Gudiksen, L. Lauhon, J. Wang, D. Smith, C. Lieber, "Growth of nanowire superlattice structures for nanoscale photonics and electronics", *Nature* 415 617-620 (2002).
[26] K. Ziegler, D. Lyons, J. Holmes, D. Erts, B. Polyakov, H. Olin, K. Svensson, E. Olsson, "Bistable nanoelectromechanical devices", *Appl. Phys. Lett*. 84 4074-4076 (2004).
[27] Z. Wang, "Towards Self-Powered Nanosystems: From Nanogenerators to Nanopiezotronics", *Adv. Funct. Mater*. 18 3553-3567 (2008).
[28] K. Liu, P. Gao, Z. Xu, X. Bai, and E. Wang, "In situ probing electrical response on bending of ZnO nanowires inside transmission electron microscope", *Appl. Phys. Lett*. 92 213105 (2008) .
[29] W. Lu, C. M. Lieber, "Semiconductor nanowires", J. Phys. D: Appl. Phys. 39, R387–R406 (2006).
[30] J. Guo, J. Wang, E. Polizzi, S. Datta, and M. Lundstrom, "Electrostatics of nanowire transistors", IEEE Trans. Nanotechnol. 2, 329 (2003).
[31] Z. H. Chen, J. Appenzeller, J. Knoch, Y. M. Lin, and P. Avouris, "The Role of Metal-Nanotube Contact in the Performance of Carbon Nanotube Field-Effect Transistors", Nano Lett . 5, 1497(2005).
[32] Z. Zhong, Y. Fang, W. Lu, and C. M. Lieber, "Coherent Single Charge Transport in Molecular-Scale Silicon Nanowires", Nano Lett. 5, 1143 (2005).
[33] H. Grabert and M. H. Devoret, "Single Charge Tunneling: Coulomb Blockade Phenomena in Nanostructures", (New York: Plenum, 1992).
[34] S. De Franceschi, J. A. van Dam, E. Bakkers, L. F. Feiner, L. Gurevich and L. P. Kouwenhoven, "Single-electron tunneling in InP nanowires", Appl. Phys. Lett. 83, 344 (2003).
[35] W. Lu, J. Xiang, B.P. Timko, Y. Wu and C.M. Lieber, "One-dimensional hole gas in germanium/silicon nanowire heterostructures", Proc. Natl. Acad. Sci. USA102, 10046-10051 (2005)
[36] E. Ozbay, "Plasmonics: Merging Photonics and Electronics at Nanoscale Dimensions", Science, 311, 189 –193 (2006).
[37] N. Engheta, "Circuits with light at nanoscales: Optical nanocircuits inspired by metamaterials", Science, 317, 1698 –1702 (2007).
[38] W. Wang, Q Yang, F. Fan, H. Xu, Z. L. Wang, "Light Propagation in Curved Silver Nanowire Plasmonic Waveguides", Nano Lett. 11, 1603–1608 (2011).
[39] D. K. Gramotnev, S. I. Bozhevolnyi, " Plasmonics beyond the diffraction limit", Nat. Photonics 4, 83 – 91 (2010).
[40] W. L. Barnes, A. Dereux, T. W. Ebbesen, "Surface plasmon subwavelength optics", Nature 424, 824 –830 (2003).

[41] H. Wei, Z. Li, X. Tian, Z. Wang, F. Cong, N. Liu, S. Zhang, P. Nordlander, N. J. Halas, and H Xu, "Quantum Dot-Based Local Field Imaging Reveals Plasmon-Based Interferometric Logic in Silver Nanowire Networks", Nano Lett. 10, 1950 –1954 (2010).
[42] J. C. Weeber, Y. Lacroute, A. Dereux, E. Devaux, T. Ebbesen, C. Girard, M. U. Gonzalez, A. L. Baudrion, "Near-field characterization of Bragg mirrors engraved in surface plasmon waveguides", Phys Rev. B 70, 235406 (2004).
[43] S. I. Bozhevolnyi, V. S. Volkov, E. Devaux, J.-Y. Laluet, and T. W. Ebbesen, "Channel plasmon subwavelength waveguide components including interferometers and ring resonators", Nature 440, 508–511 (2006).
[44] P. Neutens, P. Van Dorpe, I. De Vlaminck, L. Lagae, G. Borghs, "Electrical detection of confined gap plasmons in metal-insulatormetal waveguides", Nat. Photonics 3, 283–286 (2009).
[45] H. F. Dadgour, K. Banerjee, "Hybrid NEMS–CMOS integrated circuits: A novel strategy for energy-efficient designs", Comp. Digital Techn. 3, 593–608 (2009).
[46] O. Y. Loh and H. D. Espinosa, "Nanoelectromechanical contact switches", Nature Nanotechnol. 7, (2012).
[47] J.-P. Salvetat, A.J. Kulik, J.-M. Bonard, G.A.D. Briggs, T. Stockli, K. Metenier, S. Bonnamy, F. Beguin, N.A. Burnham, L. Forro, "Elastic modulus of ordered and disordered multiwalled carbon nanotubes", Adv. Mater. 11, 161–165 (1999).
[48] B. Wu, A. Heidelberg, J.J. Boland, "Mechanical properties of ultrahigh-strength gold nanowires", Nat. Mater. 4, 525–529 (2005).
[49] S. Shanmugham, J. Jeong, A. Alkhateeb, D.E. Aston, "Polymer nanowire elastic moduli measured with digital pulsed force mode AFM", Langmuir 21, 10214–10218 (2005).
[50] E.W. Wong, P.E. Sheehan, C.M. Lieber, "Nanobeam mechanics: elasticity, strength, and toughness of nanorods and nanotubes", Science 277,1971–1975 (1997).
[51] M.-F. Yu, O. Lourie, M. J. Dyer, K. Moloni, T.F. Kelly, and R.S. Ruoff, "Strength and breaking mechanism of multiwalled carbon nanotubes under tensile load", Science 287, 637–640 (2000).
[52] G. Feng, Y. Yong, C.J. Lee, K. Cho, W.D. Nix, "Mechanical properties of GaN and ZnO nanowires using nanoindentation", JOM 56, 35 (2004).
[53] P. Poncharal, Z.L. Wang, D. Ugarte, and W.A. de Heer, "Electrostatic deflections and electromechanical resonances of carbon nanotubes", Science 283, 1513–1516 (1999).
[54] A.V. Desai, M. A. Haque, „Mechanical properties of ZnO nanowires", Sensors and Actuators A 134, 169-176 (2007).
[55] Y. S. Zhang, Y. J. Yan, and J. Zhu, J. Chin. Electr.Microsc. Soc. 23, 483 (2004);
[56] Y. J. Yan, Y. S. Zhang,K. Q. Peng, and J. Zhu, ibid. 23, 484 (2004).
[57] A. H. Nayfeh, D. T. Mook, "Nonlinear Oscillations" (Wiley, New York, 1979).
[58] K. L. Turner, S. A. Miller, P. G. Hartwell, N. C. MacDonald, S. H. Strogatz, and S. G. Adams, "Five Parametric Resonances in a MicroElectroMechanical System", Nature 396, 149 (1998).
[59] M. F. Yu, G. J. Wagner, R. S. Ruoff, and M. J. Dyer, "Realization of parametric resonances in a nanowire mechanical system with nanomanipulation inside a scanning electron microscope", Phys.Rev. B 66, 073406 (2002).
[60] C. S. Liu and V. K. Tripathi, "Observational consequences of parametrically driven vibrations of carbon nanotubes", Phys. Rev. B 70, 115414 (2004).
[61] C. Q. Chen, Y. Shi, Y. S. Zhang, J. Zhu, and Y. J. Yan, "Size Dependence of Young's Modulus in ZnO Nanowires", PRL 96, 075505 (2006).

[62] F. Xu, Q. Qin, A. Mishra, Y. Gu, and Y. Zhu, “Mechanical Properties of ZnO Nanowires Under Different Loading Modes”, Nano Res 3 271–280 (2010).
[63] M. P. Manoharan, A. V. Desai, G . Neely, and M. A. Haque, “Synthesis and Elastic Characterization of Zinc Oxide Nanowires”, J NANOMATER. 2008 (2008).
[64] A. Sakamoto, T. Ogawa, “Effective charge in the II-VI and II-IV compounds with zincblende or wurtzite type structure,” J. Phys. Chem. Solids 36, 583–589 (1975).
[65] R. Kato and J. Hama, “First-principles calculation of the elastic stiffness tensor of aluminium nitride under high pressure”, J. Phys. Condens. Matter 6, 7617–7632 (1994).
[66] G. Stan, S. Krylyuk, A. V. Davydov, R. F. Cook, “Bending manipulation and measurements of fracture strength of silicon and oxidized silicon nanowires by atomic force microscopy”, J. Mater. Res. 27 (2012).
[67] M. C. Strus, R. R Lahiji, P. Ares, V. López, A. Raman, R. Reifenberger, “Strain energy and lateral friction force distributions of carbon nanotubes manipulated into shapes by atomic force microscopy”, Nanotechnol. 20, 385709 (2009).
[68] M. Bordag, A. Ribayrol, G. Conache, L. Fröberg, S. Gray, L. Samuelson, K. Montelius, H. Pettersson, “Shear stress measurements on InAs nanowires by AFM manipulation”, Small 3, 1398–1401 (2007).
[69] B. Polyakov, L. M. Dorogin, S. Vlassov, I. Kink, A. Lõhmus A. E. Romanov, R. Lõhmus, “Real-time measurements of sliding friction and elastic properties of ZnO nanowires inside a scanning electron microscope”, Solid State Commun. 151, 1244-1247 (2011).
[70] L. M. Dorogin, B. Polyakov, A. Petruhins, S. Vlassov, A. E. Romanov, “Modeling of kinetic and static friction between an elastically bent nanowire and a flat surface”, J. Mater. Res. 27, 580 (2011).
[71] M. H. Huang, Y. Wu, H. Feick, N. Tran, E. Weber, and P. Yang, “Catalytic Growth of Zinc Oxide Nanowires by Vapor Transport”, Adv. Mater. 13, 113–116 (2001).
[72] L. Landau, E. Lifshitz, Theory of Elasticity, (Butterworth-Heinemann, Oxford, 1986).
73 S. Timoshenko, J. N. Goodier, *Theory of Elasticity*, edn 2nd (New York: McGraw-Hill Book Company, 1951).
[74] J. Song, X. Wang, E. Riedo, Z. Wang, “Elastic Property of Vertically Aligned Nanowires”, Nano Lett. 5, 1954–1958 (2005).
[75] M. Minary-Jolandan, R. A. Bernal, I. Kuljanishvili, V. Parpoil, and H. D. Espinosa, “Individual GaN nanowires exhibit strong piezoelectricity in 3D”, Nano Lett. 12, 970-976 (2012).
[76] M. Manoharan, M. Haque, “Role of adhesion in shear strength of nanowire–substrate interfaces”, J. Phys. D: Appl. Phys. 42, 095304 (2009).
[77] Z. Zhu, T. L. Chen, Y. Gu, J. Warren, R. M. Osgood, “Zinc oxide nanowires grown by vapor-phase transport using selected metal catalysts: a comparative study”, Chem. Mater. 17 4227–4234 (2005).
[78] L. M. Dorogin, S. Vlassov, B. Polyakov, M. Antsov, R. Lõhmus, I. Kink, A. E. Romanov, Real-time manipulation of ZnO nanowires on a flat surface employed for tribological measurements: Experimental methods and modeling, Phys. Status Solidi B (2012) 1–13.
[79] Y. Ding, Z. L. Wang, “Structures of planar defects in ZnO nanobelts and nanowires”, Micron 40, 335–342 (2009).
[80] D. Dietzel, C. Ritter, T. Mönninghoff, H. Fuchs, A. Schirmeisen, U. D. Schwarz, “Frictional Duality Observed during Nanoparticle Sliding”, Phys. Rev. Lett. 101, 125505 (2008)

Non-exclusive licence to reproduce thesis and make thesis public

I, Mikk Antsov (29.12.1987),

1. herewith grant the University of Tartu a free permit (non-exclusive licence) to:

1.1. reproduce, for the purpose of preservation and making available to the public, including for addition to the DSpace digital archives until expiry of the term of validity of the copyright, and

1.2. make available to the public via the university's web environment, including via the DSpace digital archives, as of **10.09.2013** until expiry of the term of validity of the copyright,

"Tribological and mechanical characterization of ZnO nanowires",

supervised by Leonid Dorogin and Sergei Vlassov,

2. I am aware of the fact that the author retains these rights.

3. This is to certify that granting the non-exclusive licence does not infringe the intellectual property rights or rights arising from the Personal Data Protection Act.

Tartu, **23.05.2013**